Crystal Structures of Ribonuclease A Complexes with 5′-Diphosphoadenosine 3′-Phosphate and 5′-Diphosphoadenosine 2′-Phosphate at 1.7 Å Resolution[†,⊥]

Demetres D. Leonidas,[‡] Robert Shapiro,[§,||] Laurence I. Irons,[‡] Nello Russo,[§] and K. Ravi Acharya*[,‡]

School of Biology and Biochemistry, University of Bath, Claverton Down, Bath BA2 7AY, U.K., and Center for Biochemical and Biophysical Sciences and Medicine and Department of Pathology, Harvard Medical School, Boston, Massachusetts 02115

Received January 6, 1997; Revised Manuscript Received February 28, 1997[⊗]

ABSTRACT: High-resolution (1.7 Å) crystal structures have been determined for bovine pancreatic ribonuclease A (RNase A) complexed with 5′-diphosphoadenosine 3′-phosphate (ppA-3′-p) and 5′-diphosphoadenosine 2′-phosphate (ppA-2′-p), as well as for a native structure refined to 2.0 Å. These nucleotide phosphates are the two most potent inhibitors of RNase A reported so far, with K_i values of 240 and 520 nM, respectively. The binding modes and conformations of ppA-3′-p and ppA-2′-p were found to differ markedly from those anticipated on the basis of earlier structures of RNase A complexes. The key difference is that the 5′-*β*-phosphate rather than the 5′-α-phosphate of each inhibitor occupies the P_1 phosphate binding site. As a consequence, the ribose moieties of the two nucleotides are shifted by ∼2 Å compared to the positions of their counterparts in earlier complexes, and the adenine rings are rotated into unusual *syn* conformations. Thus, the six-membered and five-membered rings of both adenines are reversed with respect to the others but nonetheless engage in extensive interactions with the residues that form the B_2 purine binding site of RNase A. Despite the close structural similarity of the two inhibitors, the puckers of their furanose rings are different: C2′-*endo* and C3′-*endo*, respectively. Moreover, their 5′-α-phosphates and 3′(2′)-monophosphates interact with largely different sets of RNase residues. The results of this crystallographic study emphasize the difficulties inherent in qualitative modeling of protein−inhibitor interactions and the compelling reasons for high-resolution structural studies in which quantitative design of improved inhibitors was enabled. The structures presented here provide a promising starting point for the rational design of tight-binding RNase inhibitors, which may be used as therapeutic agents in restraining the ribonucleolytic activities of RNase homologues such as angiogenin, eosinophil-derived neurotoxin, and eosinophil cationic protein.

Bovine pancreatic ribonuclease A (RNase A;[1] EC 3.1.27.5) is one of the most extensively investigated proteins [for reviews, see Richards and Wyckoff (1971), Blackburn and Moore (1982), and Eftink and Biltonen (1987)]. It was the subject of many of the pioneering studies in protein chemistry and enzymology, involving chemical modification, refolding, amino acid sequence determination, limited proteolysis, crystallography, and peptide synthesis, among others. It has continued to be the focus of considerable attention, and a vast quantity of kinetic, mechanistic, thermodynamic, and structural information has now been collected.

Numerous studies have examined the inhibition of RNase A by small nucleotides and oligonucleotides, and crystal or NMR structures for at least a dozen complexes have been determined. Despite these efforts, no tight-binding, low-molecular weight inhibitors of this enzyme have yet been identified; indeed, the most effective small compounds reported thus far have K_i values only in the low micromolar range (Anderson et al., 1968; Irie et al., 1984; Lindquist et al., 1973). In part, this may be due to the fact that RNases have long been percieved as molecules with purely digestive functions and hence of limited biological interest or any apparent pharmaceutical benefit. In addition, the availability of an extremely potent proteinaceous inhibitor that can neutralize harmful adventitious RNases in many experimental systems [see Blackburn and Moore (1982)] may have been a factor as well.

Developments over the past decade have led to a reassessment of the role and importance of RNases, as several RNase A homologues have been demonstrated to possess potent physiological activities (D'Alessio, 1993). One of these, angiogenin (Ang) (Fett et al., 1985; Strydom et al., 1985), is an inducer of new blood vessel formation and appears to play an essential role in the growth and establish-

[†] This work is supported by the Cancer Research Campaign (K.R.A.), Wellcome Trust Biomedical Research Collaboration Grant 044107/Z/95/Z (K.R.A. and R.S.), the Endowment for Research in Human Biology, Inc., Boston (R.S. and N.R.), the National Institutes of Health (Grant HL52096 to R.S.), and the European Union through its support of the work at EMBL, Hamburg, through the HCMP Access to Large Installations Project (Contract CHGE-CT93-0400).

[⊥] The atomic coordinates for both complexes of RNase A as well as for the free structure have been deposited with the Brookhaven Protein Data Bank (accession numbers 1AFK, 1AFL, and 1AFU, respectively).

* Address correspondence to this author at the School of Biology and Biochemistry, University of Bath, Claverton Down, Bath BA2 7AY, U.K. Phone: 44-1225-826 238. Fax: 44-1225-826 779. E-mail: K.R.Acharya@bath.ac.uk.

[‡] University of Bath.

[§] Center for Biochemical and Biophysical Sciences and Medicine, Harvard Medical School.

[||] Department of Pathology, Harvard Medical School.

[⊗] Abstract published in *Advance ACS Abstracts,* April 15, 1997.

[1] Abbreviations: RNase A, bovine pancreatic ribonuclease A; Ang, angiogenin; EDN, eosinophil-derived neurotoxin; ECP, eosinophil cationic protein; ppA-3′-p, 5′-diphosphoadenosine 3′-phosphate; ppA-2′-p, 5′-diphosphoadenosine 2′-phosphate; d(CpA), deoxycytidylyl-3′,5′-adenosine; PEG, polyethylene glycol; 2′,5′-CpA, cytidylyl-2′,5′-adenosine; 5′-AMP, adenosine 5′-monophosphate; 2′-CMP, cytidine 2′-monophosphate.

S0006-2960(97)00033-0 CCC: $14.00

ment of multiple types of human tumors (Olson et al., 1994, 1995). Mutational studies have demonstrated that the angiogenic action of Ang is critically dependent on its ribonucleolytic activity (Shapiro et al., 1989; Shapiro & Vallee, 1989). Two other homologues, eosinophil-derived neurotoxin (EDN) and eosinophil cationic protein (ECP) (Gleich et al., 1986), are neurotoxic *in vivo* and are thought to produce some of the neurological symptoms associated with eosinophilia-myalagia and hypereosinophilia syndromes. Like Ang, EDN and ECP may utilize their ribonucleolytic activities to elicit their physiological effects (Sorrentino et al., 1992). Thus, the enzymatic active sites of these proteins are attractive targets for new therapeutic agents. Moreover, RNase inhibitors may be useful for exploration of the biological mechanism of these molecules.

Efforts toward the design of potent small inhibitors of these and other biologically active RNase superfamily enzymes have been initiated (Russo et al., 1997) and have focused on RNase A for several reasons. First, the amount of structural and functional information available on this enzyme makes it an obvious choice as a model system. Second, RNase A complexes have already proved to be quite amenable to crystallographic studies; in contrast, crystals of Ang complexes have not been obtained thus far, the structure of native EDN has only recently been described (Mosimann et al., 1996), and structural work on ECP has yet to be reported. Third, the catalytic centers of Ang and EDN appear to be fairly similar to that of RNase A (Acharya et al., 1994; Mosimann et al., 1996), suggesting that RNase A inhibitors might also be effective against these other proteins or that they can be tailored for this purpose. Finally, small-molecule RNase A inhibitors themselves would have practical value, since the protein inhibitor is unstable and is irreversibly inactivated under denaturing or oxidizing conditions (Blackburn & Moore, 1982).

The active site of RNase A contains numerous subsites for binding the various phosphate, base, and ribose moieties of the RNA substrate. These sites, designated $P_o\cdots P_n$, $B_o\cdots B_n$, and $R_o\cdots R_n$, respectively, are shown schematically in Figure 1 (Richards & Wyckoff, 1971; Parés et al., 1991). The three central sites are P_1, where P−O5′ bond cleavage occurs; B_1, which interacts with the base whose ribose contributes its 3′-oxygen to the scissile phosphodiester bond; and B_2, which binds the base whose ribose provides the 5′-oxygen. B_1 has a nearly absolute specificity for pyrimidines, whereas B_2 strongly prefers purines.

Two new RNase A inhibitors, 5′-diphosphoadenosine 3′-phosphate (ppA-3′-p) and 5′- diphosphoadenosine 2′-phosphate (ppA-2′-p), have recently been synthesized (Russo et al., 1997). They are the most potent nucleotide ligands identified thus far, with K_i values of 240 and 520 nM, respectively, at pH 5.9. Both compounds were expected to occupy the P_1, B_2, R_2, and P_2 subsites of RNase, engaging in a large number of favorable interactions. In the present study, high-resolution (1.7 Å) crystal structures of the two complexes reveal that ppA-3′-p and ppA-2′-p indeed interact with the region predicted, but their binding modes differ strikingly from those anticipated on the basis of previous RNase complex structures. These findings have important implications for RNase inhibitor development as well as for rational design efforts in general.

EXPERIMENTAL PROCEDURES

Diffraction Measurements. Bovine pancreatic RNase A was obtained from Sigma (type XII-A). The inhibitors ppA-3′-p and ppA-2′-p were prepared as described (Russo et al., 1996, 1997). RNase A crystals were grown using the hanging drop vapor diffusion method. Drops containing protein (10 mg/mL) at pH 5.5 in 10 mM sodium citrate buffer and 10% PEG 4000 were equilibrated against reservoirs containing 20% PEG 4000 and 20 mM sodium citrate buffer at pH 5.5. Single crystals appeared after 7−10 days at 16 °C. Cocrystals of the RNase A complex with ppA-3′-p were grown under the same conditions as those for free enzyme, but in the presence of 0.5 mM inhibitor. The RNase crystals diffract to minimum Bragg spacings of 1.7 Å using synchrotron radiation. The systematic absences and symmetry were consistent with space group *C*2 with the following unit cell dimensions: $a = 101.54$ Å, $b = 33.36$ Å, $c = 73.25$ Å, and $\beta = 90.09°$. Since the β angle is close to 90°, initially, diffraction data were processed in C-centered orthorhombic space group *C*222, but the resulting R_{sym} was 0.40, for monoclinic space group *C*2, it was 0.044. This ruled out the possibility that the chosen space group is not absolutely correct. There are two molecules of RNase per crystallographic asymmetric unit, and approximately 48% of the crystal volume is occupied by solvent. Soaking experiments were performed at 16 °C with 10 mM ppA-2′-p for 3 h (RNase A−ppA-2′-p complex) or with 1 mM ppA-3′-p for 2.5 h (RNase A−ppA-3′-p complex). Prior to soaking, RNase crystals were stabilized in a solution containing 20 mM sodium citrate buffer at pH 5.5 with 25% PEG 4000 for at least 24 h. K_i values for these nucleotides measured under the soaking conditions are similar to those reported by Russo et al. (1997).

Diffraction data were collected on station PX 9.6 ($\lambda = 0.87$ Å), of the Synchrotron Radiation Source, Daresbury, U.K., for free RNase at 2.0 Å resolution and for the RNase A−ppA-2′-p complex at 1.7 Å resolution using a 30 cm diameter MAR-research image plate (crystal to image plate distance of 158 mm). Diffraction data for the RNase−ppA-3′-p complex at 1.7 Å resolution were collected at EMBL beamline X31 ($\lambda = 0.92$ Å) located at HASYLAB, DESY Hamburg, using an 18 cm diameter MAR-research image plate (crystal to image plate distance of 148 mm). One crystal per data set was used (at 16 °C) with an oscillation range of 1.5°/image, and 100° of data were collected for each data set to minimize the "missing cone" of data. Additional data at low resolution (2.5 Å) for the RNase−ppA-2′-p complex (10 mM) were collected for one crystal, on a Siemens area detector mounted on a Siemens rotating anode X-ray source with CuKα radiation operating at 46 kV and 70 mA. Overall, 846 frames of data were collected with an oscillation range of 0.25°/frame, a crystal to detector distance of 110 mm, a 2θ angle of 15°, and 130 s per frame exposure.

Data Processing and Reduction. Raw data images were indexed, integrated, and corrected for Lorentz and polarization effects using the program DENZO (Otwinowski, 1993). All data were scaled and merged using the program SCALEPACK (Otwinowski, 1993). The XDS program (Kabsch, 1988) was used for raw area detector data processing and reduction. Intensity measurements for the RNase A−ppA-2′-p complex from the area detector and the synchrotron were merged and scaled by the SCALA program

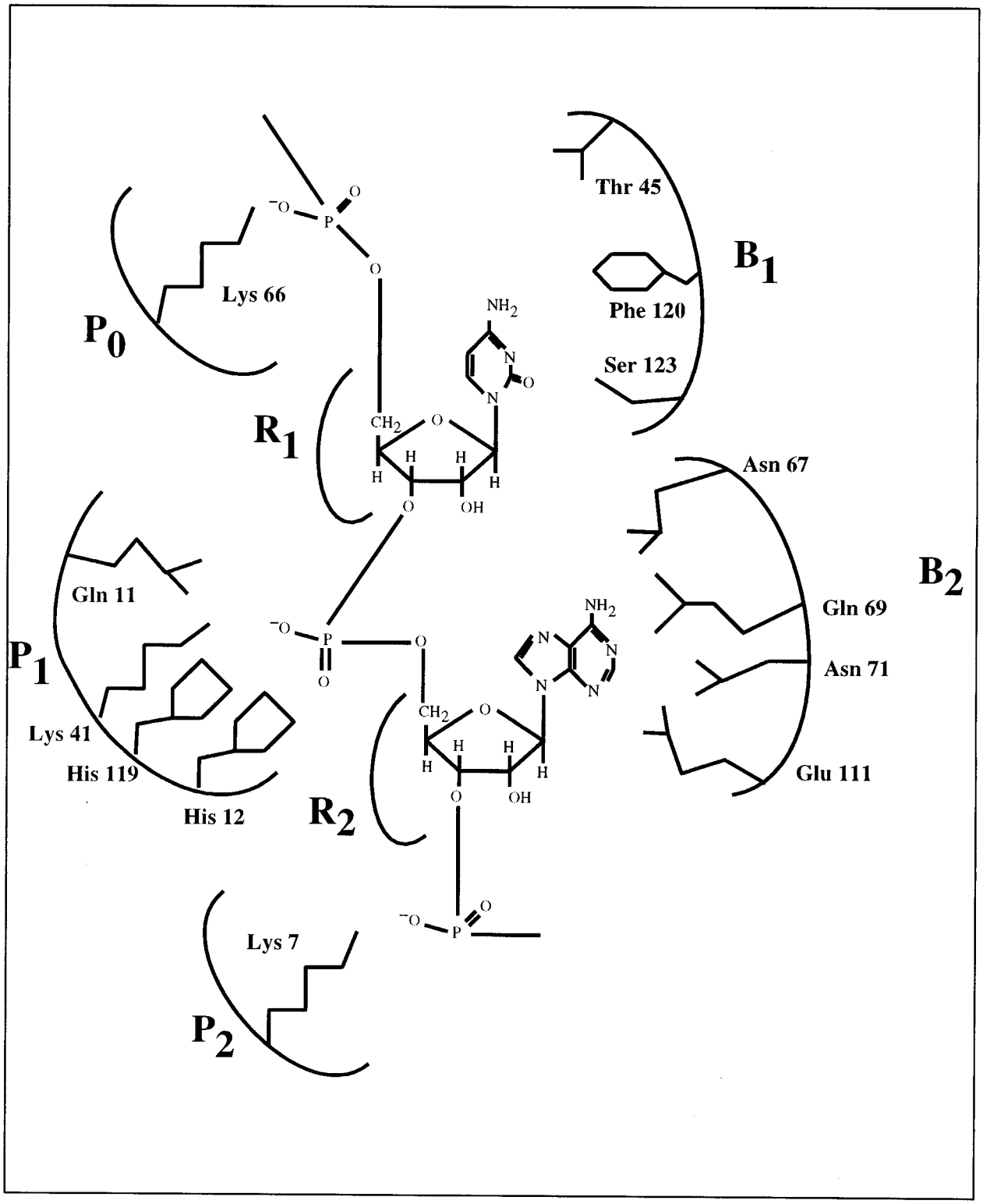

FIGURE 1: Schematic diagram of the subsites of the RNase A active site, adapted from Parés et al. (1991). The residues shown were seen in various crystal and NMR structures to be within the sites.

(CCP4, Bailey, 1994). Intensities were truncated to amplitudes by the TRUNCATE program (French & Wilson, 1978). The details of data processing statistics for the three data sets are presented in Table 1.

Phasing. The native structure of RNase A was determined by the method of molecular replacement using the program AMoRe (Navaza, 1994) with the coordinates of native RNase A at 1.45 Å resolution [PDB 3RN3 (Howlin et al., 1989)] as a search model. Data in the range of 10−3.5 Å were used for both the rotation and the translation function searches. Using a Patterson cutoff radius of 26 Å, a list of 100 rotation function peaks was obtained with the top peak having a correlation coefficient of 9.5 (5.3σ above the mean). The translation function gave two peaks with correlation coefficients of 22.9 and 22.0 (16.4σ and 15.7σ above the mean, respectively). The correlation coefficients for the two solutions increased to a value of 65.7 after rigid-body refinement with AMoRe, and the R factor was 33.7%. No

Table 1: X-ray Data Collection and Refinement Statistics

	native	ppA-3′-p complex	ppA-2′-p complex
Data Collection Statistics			
resolution (Å)	30.0−2.0	30.0−1.7	30.0−1.7
reflections measured	38 250	73 892	87 383
unique reflections	15 331	24 687	25 897
completeness (outermost shell) (%)	89.6 (79.5)	91.4 (82.4)	93.1 (89.2)
$I/\sigma I$	18.1	9.2	9.9
multiplicity	2.5	3.0	3.4
R_{sym}[a] (%)	4.4	5.7	9.0
Refinement Statistics			
resolution (Å)	8.0−2.0	8.0−1.7	8.0−1.7
R_{cryst}[b] (%)	20.1	21.1	21.7
R_{free}[c] (%)	28.5	26.6	27.8
number of reflections	15 149	24 566	25 600
number of protein atoms	1894	1902	1901
number of ligand atoms	−	62	62
number of water molecules per dimer	83	162	122
number of citrate molecules	−	−	2
deviations from ideality (rms)			
bond lengths (Å)	0.012	0.009	0.009
bond angles (deg)	1.7	1.4	1.5
dihedrals (deg)	25.3	25.0	25.1
impropers (deg)	1.4	1.2	1.3
average B factor (Å^2)			
main chain atoms	18.9	19.4	20.8
side chain atoms	22.2	22.1	23.2
all protein atoms	20.5	20.7	21.9
solvent atoms	32.7	37.0	34.6
ligand atoms (molecule I/molecule II)	−	30.9/40.6	38.9/47.1

[a] $R_{sym} = \sum_h\sum_i|I(h) - I_i(h)|/\sum_h\sum_i I_i(h)$, where $I_i(h)$ and $I(h)$ are the ith and the mean measurements of the intensity of reflection h, respectively. [b] $R_{cryst} = \sum_h|F_o - F_c|/\sum_h F_o$, where F_o and F_c are the observed and calculated structure factor amplitudes of reflection h, respectively. [c] R_{free} is equal to R_{cryst} for a randomly selected 5% subset of reflections not used in the refinement (Brünger, 1992b).

solution was found using space group $C222$ instead of $C2$.

Refinement. The output model from AMoRe, which comprised two molecules of RNase, was subjected to rigid-body refinement with X-PLOR (Brünger, 1992a) using data from 10 to 3.5 Å. The R_{free} (Brünger, 1992b) at this stage was 36.5% and the conventional R_{cryst} 18.6%. This model was used as a starting point for each one of the three data sets (one for free RNase A and two for the RNase A−inhibitor complexes). Alternating cycles of manual building, conventional positional refinement, and the simulated annealing method as implemented in X-PLOR improved the model. Rebuilding was initially performed at 3.5 Å resolution using the interactive computer graphics program O version 5.10.3 (Jones et al., 1991) implemented on an Indigo^2 Silicon Graphics workstation. Extension of refinement from 3.5 to 2.0 Å resolution for the native structure or from 3.5 to 1.7 Å resolution for each RNase A−inhibitor complex was performed in 0.1 Å resolution steps, and the quality of the model was monitored using SigmaA-weighted $2|F_o| - |F_c|\phi_{calc}$ maps calculated using the program SIGMAA (Read, 1986). The behavior of the R_{free} value was also monitored throughout the refinement. The inhibitor molecule was included during the final stages of the refinement by using part of the atomic coordinates of NADPH from the crystal structure of the dihydrofolate reductase−NADPH complex [PDB 3DFR (Filman et al., 1982)] which was consistent with the chemical formula of the inhibitors as a starting structure. The inhibitor molecule was initially fitted using the $|F_o| - |F_c|$ maps, and subsequent fitting was performed into $2|F_o| - |F_c|$ inhibitor complex maps. During the final stages of refinement, after the inclusion of the inhibitor molecule, water molecules were inserted into the model only if there were peaks in the $|F_o| - |F_c|$ electron density maps with heights greater than 3σ and they were at hydrogen bond-forming distances from appropriate atoms. The $2|F_o| - |F_c|\phi_{calc}$ maps were also used to check the consistency in peaks. Water molecules with a temperature factor higher than 60 Å^2 were excluded from subsequent refinement steps. Noncrystallographic symmetry restraints were applied for the RNase molecules as well as for the inhibitor molecules throughout the refinement procedure, tight at the beginning and more relaxed toward the end, and finally, they were released in the final refinement cycle. The details of refinement statistics for the three structures are listed in Table 1.

The program PROCHECK (Laskowski et al., 1993) was used to assess the quality of the final structures. Analysis of the Ramachandran ($\varphi-\psi$) plot for the three structures showed that all residues lie in the allowed regions except Ser 22 in one of the two RNase molecules in the free structure which lies in a generously allowed region. This residue is modeled as alanine in the RNase A−ppA-2′-p complex structure due to insufficient electron density for the side chain.

RESULTS AND DISCUSSION

Overall Structures. The structures of RNase A reported here are very similar to those reported previously and in particular, to two high-resolution native structures, one at 1.45 Å [PDB 3RN3 (Howlin et al., 1989)] and another at 1.26 Å [PDB 7RSA (Wlodawer et al., 1988)]. The rms differences between these two earlier structures and the present free RNase A structure are 0.42/0.52 and 0.40/0.49 Å (molecule 1/molecule 2 of the RNase A noncrystallographic dimer) for 3RN3 and 7RSA, respectively. The corre-

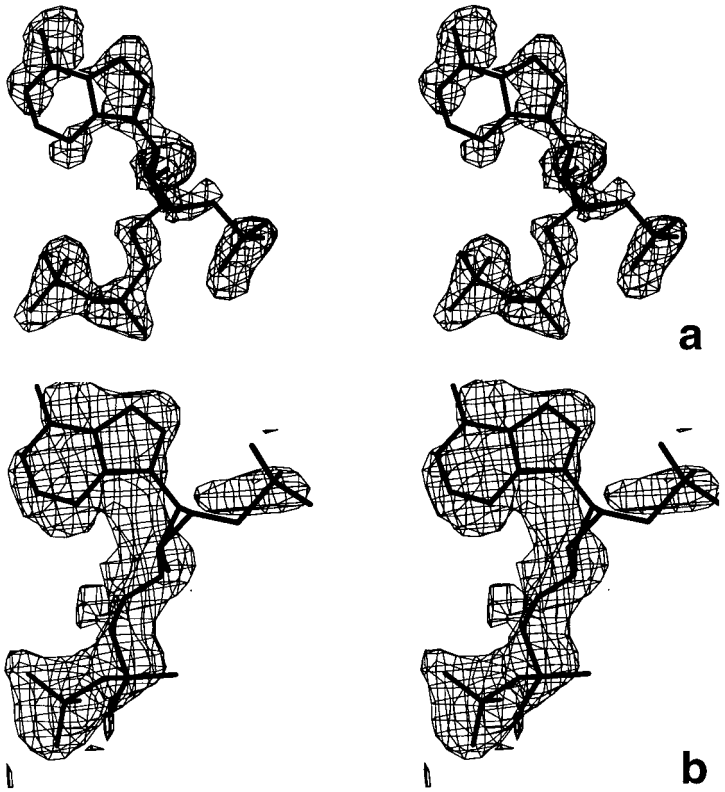

FIGURE 2: A stereo diagram of a simulated annealing omit 1.7 Å $|F_o| - |F_c|$ electron density map calculated using the standard protocol as implemented in X-PLOR 3.851 (Hodel et al., 1992; Read et al., 1986) and omiting (a) the ppA-3′-p and (b) the ppA-2′-p inhibitors from the model coordinates to avoid any bias. The map is contoured at the 3.0σ level. The refined structures of (a) ppA-3′-p and (b) ppA-2′-p are shown. The figure was generated using the program O (Jones et al., 1991).

sponding values for the rms differences for the RNase A−ppA-3′-p complex are 0.40/0.51 and 0.40/0.48 Å, respectively, and for the RNase A−ppA-2′-p complex are 0.39/0.52 and 0.38/0.49 Å, respectively. Most of the amino acid residues in all three new structures are very well defined in the electron density map with the exception of the loop region between residues 16 and 24, which has high temperature factors and appears to be disordered. Portions of the electron density maps (at 1.7 Å) for the active site of the ppA-3′-p and ppA-2′-p complexes are shown in Figure 2. The side chain of His 119 is found in two conformations (A and B) in the free RNase structure as observed in previous structures (Borkakoti et al., 1982; Zegers et al., 1994). The occupancy appears to be 0.7 for conformation A and 0.3 for conformation B, in accord with previous studies on RNase A crystallized at pH 5.5 (deMel et al., 1995). In both complexes, the imidazole ring of this histidine is only in conformation A since conformation B is incompatible with inhibitor binding. Asp 83 and Arg 85 are also found to have two conformations as in some previous studies (deMel et al., 1995; Kim et al., 1992). The catalytic site in the free RNase structure is occupied by eight water molecules which are involved in a network of hydrogen bonds involving Ala 4, Gln 11, His 12, Gln 69, Asn 71, Val 118, and Phe 120. The exact positioning of the inhibitor bound to the RNase A molecule is shown in Figure 3. The packing of the noncrystallographic dimer in all three structures is identical to that observed in the structure of RNase B (a glycosylated form of the enzyme), also from monoclinic crystals (Williams et al., 1987). The two monomers are almost perpendicular to each other; the interface between them consists on one side of an α-helix (residues 51−59), a β-strand (residues 60−63), and a loop region (residues 75−79) from one molecule, while on the other side it contains an α-helix (residues 1−13), a loop region (residues 14−17), and the end of an α-helix (residues 32−34) from the other molecule. In the free RNase A structure, there are 22 water molecules in the dimer interface, and four of them mediate interactions between the two monomers. In the structure of the RNase

FIGURE 3: Schematic representation of the RNase A−ppA-3′-p complex. The diagram was drawn with MOLSCRIPT (Kraulis, 1991).

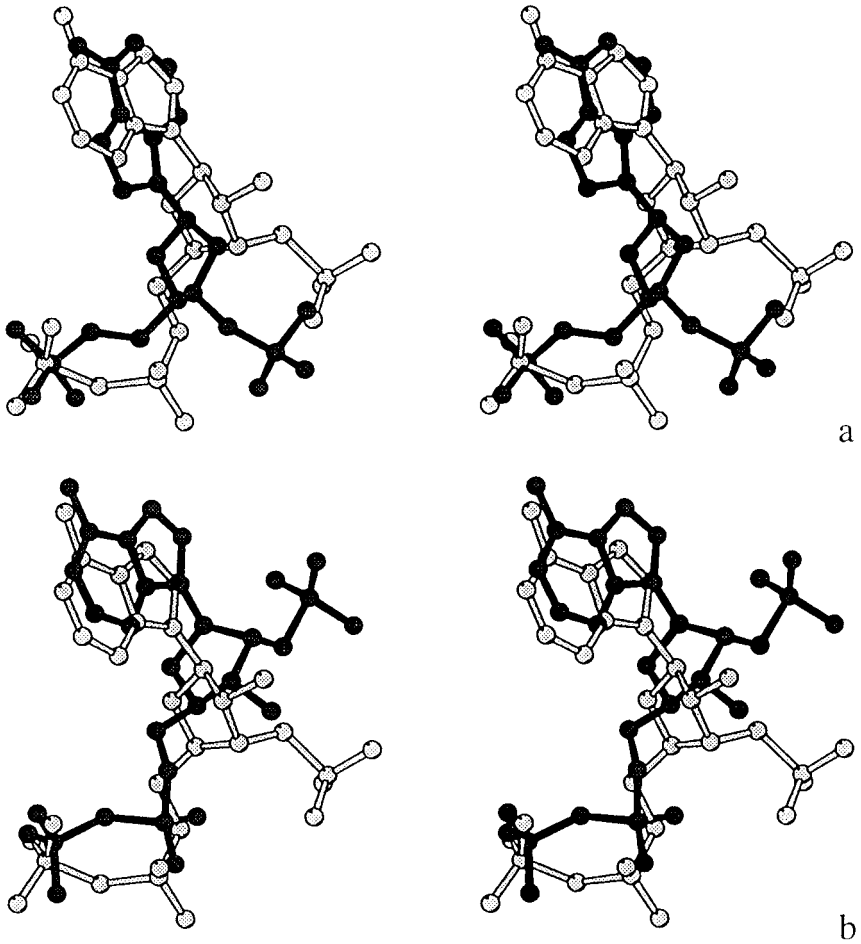

FIGURE 4: Stereoview of the superimposed structures of (a) ppA-3′-p (black) and the adenine part of d(ApTpApA) (gray) (Fontecilla-Camps et al., 1994) and (b) ppA-3′-p (black) and ppA-2′-p (gray) when bound to RNase.

A−ppA-2′-p complex, there are 29 water molecules in the interface, while in the RNase A−ppA-3′-p complex, there are 35; however, but in both cases, there are again four water molecules which mediate interactions between the two protein molecules. The active site is accessible in both molecules.

The rms differences between the two monomers are 0.46 Å for free RNase, 0.41 Å for the RNase−ppA-3′-p complex, and 0.40 Å for the RNase−ppA-2′-p complex. Differences occur primarily in the loop regions. The active sites of the two monomers with the exception of Lys 7 are identical in all three structures.

The rms differences between the structures of free RNase A and the ppA-3′-p and ppA-2′-p complexes are 0.24 and 0.32 Å, respectively, while the rms difference between the structures of the two complexes is 0.23 Å. The differences between the three structures of RNase are concentrated in the loop regions and especially in the regions between residues 36 and 40, 66 and 69, and 87 and 94. These regions are also more variable in other RNase A structures (Zegers et al., 1994), and the differences do not seem to be related to the presence or absence of an inhibitor. The free RNase structure, determined at 2.0 Å resolution, contains 83 water molecules. The structures of the ppA-3′-p and ppA-2′-p complexes are determined to a higher resolution (1.7 Å) and contain 162 and 122 water molecules, respectively. Also, two molecules of citrate, which was included in the crystallization medium, are observed in the RNase A−ppA-2′-p complex. The residues in the active site are oriented similarly in all three structures, and with the exception of His 119 (noted above) and Lys 7, no changes are observed in response to inhibitor binding. Lys 7 occupies significantly different positions in all three structures, and it appears that its position is determined by the interactions available for the amino group of its side chain.

Structures of Inhibitors when Bound to RNase A. The electron density for the inhibitor ppA-3′-p is of high quality, and all atoms are well-defined in both molecules (full occupancy) of the noncrystallographic dimer (molecule I is shown in Figure 2a). In the ppA-2′-p complex, the electron density for molecule II is well-defined for most of the atoms (full occupancy), except for the 2′-phosphate and part of the ribose (Figure 2b). For molecule I, however, the density is relatively poor (occupancy 0.6) and most of the atoms have high temperature factors (Table 1). Hence, only molecule II of this complex will be considered throughout our discussion.

The conformation of adenosine in the ppA-3′-p−RNase A complex differs considerably from those observed previously for B_2-bound adenosines in the complexes of RNase A with d(ApTpApA) (Fontecilla-Camps et al., 1994; PDB 1RCN), d(CpA) (Zegers et al., 1994; 1RPG; Toiron et al., 1996) (Figure 4), and cytidylyl-2′,5′-adenosine (2′,5′-CpA) (Toiron et al., 1996), as well as those encountered most frequently in free adenosine nucleotides. In the following discussion, references to the preferred conformations of protein-bound and free nucleotides are based on the study by Moodie and Thornton (1993). Particularly unusual is the

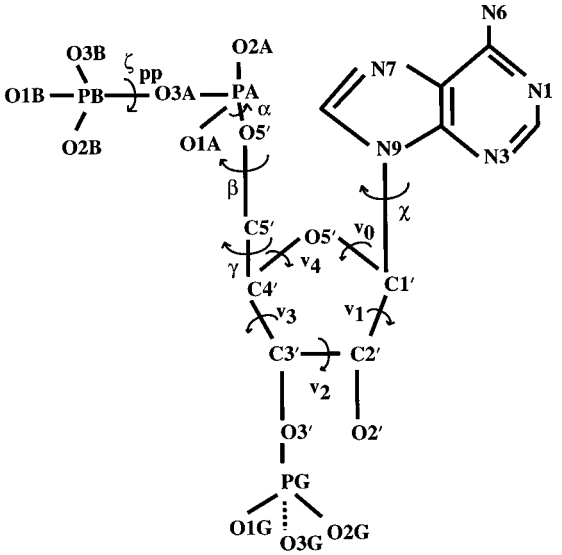

FIGURE 5: Numbering scheme and torsional angle assignment for ppA-3′-p (Moodie & Thornton, 1993).

Table 2: Torsion Angles for ppA-3′-p and ppA-2′-p when Bound to RNase A[a]

	ppA-3′-p		ppA-2′-p
torsion angles (deg)	molecule I	molecule II	molecule II
backbone torsion angles			
O5′−C5′−C4′−C3′ (γ)	−71 (*−sc*)	−67 (*−sc*)	−63 (*−sc*)
C5′−C4′−C3′−O3′ (δ)	148	150	88
C5′−C4′−C3′−C2′	−95	−88	−151
C4′−C3′−C2′−O2′	−159	−174	−64
glycosyl torsion angle			
O4′−C1′−N9−C4 (χ)	75 (*syn*)	80 (*syn*)	33 (*syn*)
pseudorotation angles			
C4′−O4′−C1′−C2′ (υ_0)	−40	−46	−2
O4′−C1′−C2′−C3′ (υ_1)	52	66	−25
C1′−C2′−C3′−C4′ (υ_2)	−42	−61	40
C2′−C3′−C4′−O4′ (υ_3)	21	37	−46
C3′−C4′−O4′−C1′ (υ_4)	12	7	29
phase	147	156	23
	C2′-endo	*C2′-endo*	*C3′-endo*
phosphate torsion angles			
O3A−PA−O5′−C5 (α)	63	47	−58
PA−O5′−C5′−C4′ (β)	161	125	−98
PG−O2′−C2′−C1′	−	−	83
PG−O2′−C2′−C3′	−	−	−175
PG−O3′−C3′−C4′	−107	−134	−
PG−O3′−C3′−C2′	143	126	−
PB−O3A−PA−O5′ (ζ_{pp})	−82	66	−109

[a] Definitions of the torsion angles are according to the current IUPAC-IUB Joint Commission on Biochemical Nomenclature (1983), and the phase angle of the ribose ring is calculated as described by Altona and Sundaralingam (1972).

orientation about the C4′−C5′ bond (γ torsion angle), which is in the *−sc* range (Figure 5, Table 2). In the d(ApTpApA) and 2′,5′-d(CpA) complexes, γ is in the *+sc* range, as is generally the case in solution. In the d(CpA) complex, γ is in the *ap* region commonly found with protein-bound polynucleotides. Both *−sc* and *ap* are extended conformations that orient the 5′-phosphate away from the adenosine. The *syn* glycosyl torsion angle χ in ppA-3′-p is also quite atypical; the B_2 adenosines in the d(ApTpApA), d(CpA), and 2′,5′-d(CpA) complexes adopt *anti* conformations, as do virtually all free adenosine derivatives examined. The χ angle in ppA-3′-p in fact differs by almost 180° from those in the other RNase-bound inhibitors, making this part of the nucleotide more compact.

Table 3: Hydrogen Bond Interactions between Inhibitors and RNase A[a]

		ppA-3′-p		ppA-2′-p
inhibitor atom	RNase A atom	molecule I	molecule II	molecule II
O1A	Lys 7 Nζ	−	2.9	3.1
	Gln 11 Nϵ2	3.1	2.7	−
	water	−	−	2.4
O2A	Lys 7 Nζ	−	3.3	2.7
O3A	Gln 11 Nϵ2	2.9	−	−
	water	3.3	−	3.0
O1B	His 12 Nϵ2	2.8	3.3	2.7
	Phe 120 N	3.0	2.8	2.9
	water	2.7	2.4	2.7
O2B	Gln 11 Nϵ2	−	−	3.1
	His 12 Nϵ2	−	2.7	−
	Lys 41 Nζ	2.9	−	−
	water	2.7	−	2.9
O3B	His 119 Nδ1	2.6	2.6	2.5
	water	3.2	−	−
O1G	Lys 7 Nζ	2.7	2.7	−
O5′	Lys 7 Nζ	3.3	2.8	−
	water	−	2.8	−
N1	water	2.6	3.1	3.1
N6	Asn 67 Oδ1	3.3	−	3.2
	Gln 69 Oϵ1	−	2.8	−
	Asn 71 Oδ1	3.0	2.4	3.0
N7	Asn 71 Nδ2	3.3	−	2.9

[a] Numbers in columns are distances in angstroms. Hydrogen bonds are listed if the distance between a donor (D) and an acceptor (A) is shorter than 3.3 Å and if the angle D−H−A is greater than 90°. For the RNase−ppA-2′-p complex, hydrogen bond interactions are listed only for molecule II since the occupancy for the inhibitor in molecule I of the noncrystallographic dimer is low.

Other aspects of the ppA-3′-p conformation more closely resemble previous patterns. The pucker of the furanose ring in ppA-3′-p is *C2′-endo*, one of the two most frequently observed ribose conformations in both protein-bound and free adenosine nucleotides (the other is *C3′-endo*). The adenosine sugar in the d(CpA) complex is also *C2′-endo* [Toiron et al., 1996; Zegers et al. (1994), where it is reported as *C2′-exo*]. The orientation of the 3′-phosphate in ppA-3′-p, as indicated by the torsion angles δ and ϵ, is well within the normal range. Finally, the 5′-phosphate torsion angle β is quite similar to those in previous complexes (161 vs 146−164°).

The conformation of bound ppA-2′-p bears a strong overall resemblance to that of ppA-3′-p; again, the glycosyl torsion angle and the orientation about the C4′−C5′ bond are in the unusual *syn* and *−sc* ranges, respectively (Figure 4). Moreover, the positions of the adenine ring and terminal 5′-phosphate with respect to each other are nearly the same. These two moieties are critical anchoring points in the interactions of both inhibitors with RNase (see below). However, there are also noteworthy differences between the two structures. The furanose pucker of ppA-2′-p is *C3′-endo* rather than *C2′-endo*; this conformation is observed in the d(ApTpApA) and 2′,5′-d(CpA) complexes as well. In addition, the orientations of the pyrophosphate groups in the two complexes are quite distinct, as reflected in the torsion angles α and β, which differ by 120−160°.

Interactions of Inhibitors with RNase A. There are striking differences between the interactions of ppA-3′-p and ppA-2′-p with RNase A (Table 3) and those anticipated on the basis of earlier structures of complexes with 5′-AMP (Richards et al., 1972), d(CpA) (Zegers et al., 1994), 2′,5′-CpA (Toiron et al., 1996), and d(ApTpApA) (Fontecilla-

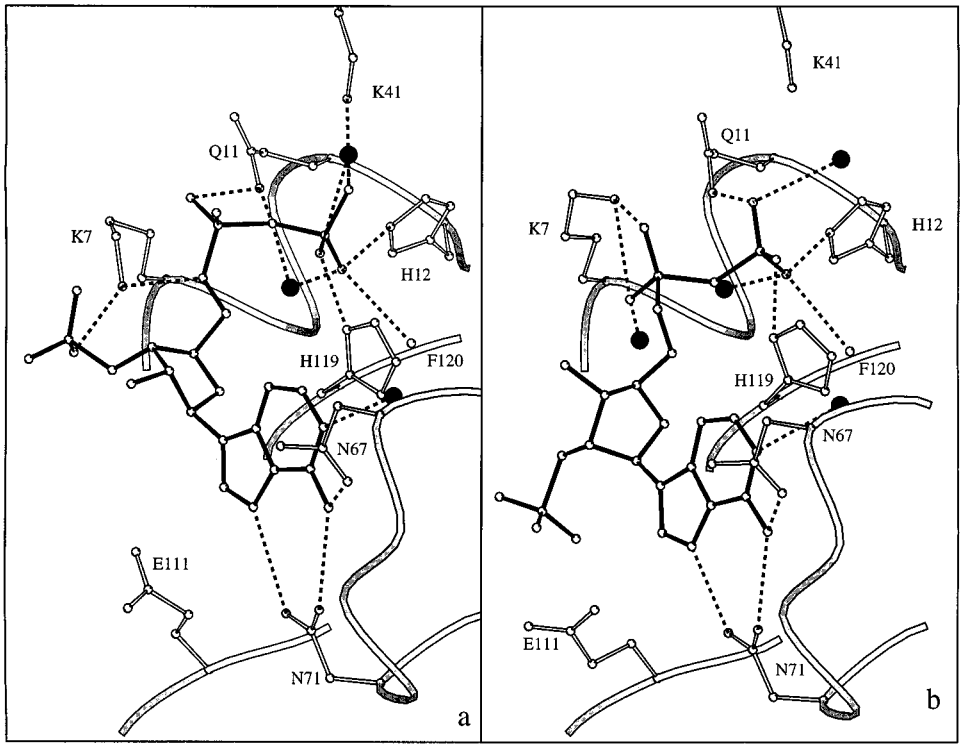

FIGURE 6: Interactions of the inhibitor molecules and RNase A: (a) ppA-3′-p and (b) ppA-2′-p. RNase residues are drawn as ball-and-stick models and water molecules as black spheres, and the inhibitor molecules are shown in black. Hydrogen bonds are indicated by dashed lines. Diagrams were drawn with MOLSCRIPT (Kraulis, 1991).

Camps et al., 1994). The key difference is at the P_1 subsite, where in all previous complexes the 5′-phosphate of the B_2 site adenosine was seen to bind. With both ppA-3′-p and ppA-2′-p, the β- rather than the α- phosphate occupies this site. Indeed, each β-phosphate forms the same extensive set of hydrogen bonds with the main chain N of Phe 120 and the side chains of His 12 and His 119 (Figure 6a,b) as do the P_1 phosphates in the complexes of RNase with d(ApTpApA), d(CpA), 2′-CMP (Howlin et al., 1987; Lisgarten et al., 1993), and 3′-CMP (Zegers et al., 1994). Other hydrogen bonds of the P_1 phosphate in some earlier complexes (e.g., with Gln 11 or Lys 41) are also replicated in the ppA-3′-p or ppA-2′-p complex. Superpositions of these various structures reveal that the Pβ atoms in the ppA-3′-p and ppA-2′-p complexes and the P_1 phosphorus atoms in the earlier complexes all lie within 0.1−0.7 Å of each other (Figure 4). Despite the similarity of the positions of the 5′-β-phosphates in the ppA-3′-p and ppA-2′-p complexes, the Pα atoms in the superimposed structures are separated by 1.5 Å and the phosphates form different interactions with RNase. In the ppA-3′-p complex, hydrogen bonds connect O1A to Nϵ2 of Gln 11 and O5′ to Nζ of Lys 7, whereas in the ppA-2′-p complex, both O1A and O2A hydrogen bond with Lys 7 Nζ (Figure 6a,b).

The placement of the β- rather than the α-phosphates in the P_1 site requires that the ribose and adenine moieties of these nucleotides be oriented quite differently from their counterparts in the other complexes. In both cases, the ribose is shifted ∼2 Å farther away from P_1 and the adenine ring is rotated by ∼180°. A consequence of these two features is that the adenines in ppA-3′-p and ppA-2′-p occupy essentially the same B_2 site space as those in the earlier complexes and are almost coplanar with them, but their six- and five-membered rings are reversed with respect to the others (Figure 4). The adenines in the ppA-3′-p and ppA-2′-p complexes superimpose reasonably well, with an rms difference of 1.0 Å. Only N6 has a position similar to those in the earlier structures and can interact with some of the same RNase residues. In all of the complexes, this amino group hydrogen bonds with Oδ1 of Asn 71. Additional hydrogen bonds with Oδ1 of Asn 67 and/or Oϵ1 of Gln 69 are seen in some of the complexes (Figure 6a,b). The sulfur atom of Cys 65 is also within hydrogen bonding distance of N6 in the ppA-3′-p and ppA-2′-p complexes, 3.1 and 2.8 Å, respectively. N7 in the two inhibitors corresponds in position to N1 in the others and interacts with the same RNase residue substituent, Nδ2 of Asn 71.

In the d(ApTpApA) and d(CpA) complex structures, the His 119 imidazole stacks against the five-membered ring of adenine; in each case, the planes of the two rings are ∼4.0 Å apart and parallel, and the rings line up well, with no significant offset. The rotation of adenine in the ppA-3′-p and ppA-2′-p complexes replaces this stacking interaction with one between the six-membered ring of adenine and the His 119 imidazole that has a somewhat different geometry; i.e., the planes of the two aromatic rings are now slightly off-parallel, and the rings are offset by ∼0.4 Å. Moreover, the average distance between the two components is even shorter, ∼3.5 Å. In addition to the hydrogen bonds and stacking interactions between RNase and the adenines of both ppA-3′-p and ppA-2′-p, there are also numerous van der Waals contacts involving Cys 65, Asn 67, Gln 69, Asn 71, Ala 109, Glu 111, and Val 118.

The ribose moieties associated with the adenines in ppA-3′-p and ppA-2′-p have different puckers (see above), and their C2′/C3′ sides deviate by about 2 Å. The O4′/C4′ sides of the rings are closer in position and in both cases pack closely against the carbonyl oxygen of Val 118 and Cβ of His 119. In fact, the separation between O4′ and the latter atom, 2.7−3.0 Å, is significantly shorter than the van der

Waals contact distance of 3.4−3.6 Å, perhaps indicating that the interaction is a nontraditional CH···O hydrogen bond. The existence of such bonds in proteins is documented [see Burley and Petsko (1988)] although uncommon.

The 3′-phosphate of ppA-3′-p points away from the adenine moiety and interacts with RNase A through a 2.7 Å hydrogen bond to Nζ of Lys 7 (Figure 6a). This lysine interacts with the corresponding phosphate in the d(ApT-pApA) complex and is generally considered to be a component of the P_2 subsite (Parés et al., 1991). This retention of function, however, requires considerable movement of the side chain (3.5 Å for Nζ) since the locations of the phosphate groups in the two structures differ greatly, due to the shift in the overall ribose position as well as the changed furanose pucker. In the ppA-2′-p complex, Lys 7 is too far removed from the 2′-phosphate to allow any interaction and instead moves to a third position [3.1 and 2.5 Å from those in the ppA-3′-p and d(ApTpApA) complexes, respectively] where, as already noted, it hydrogen bonds to O5′ (Figure 6b).

Neither 2′-hydroxyl of ppA-3′-p in the dimeric unit contacts any RNase residue within the same noncrystallographic dimer, but O2′ of molecule I hydrogen bonds to Thr 70 Oγ1 of a symmetry-related molecule. This intermolecular interaction apparently does not influence the mode of binding, since there are no significant differences between the two molecules.

The 2′-phosphate of ppA-2′-p points toward the adenine moiety and occupies the space close to the carboxyl group of Glu 111, with several O−O distances of <3.3 Å. However, the phosphate is highly mobile, and its orientation is not well-fixed. The electron density for this group is rather poor (Figure 2b). The observed conformation is a time and space average of an ensemble of positions which this group could occupy. It is therefore unclear whether there are any favorable contacts between the two groups. Electrostatic repulsion would most likely prevent such an interaction at neutral or alkaline pH (where both groups are fully deprotonated) unless a compensating cation is also present. At pH 5.5 which was used for soaking the RNase crystals with inhibitor, the phosphate would presumably be largely a mono- rather than a dianion, and the Glu carboxyl may also be partially protonated since its normal pK_a of ∼4.5 may well be shifted upward by the proximity of the phosphate anion. Thus, it is theoretically possible that the two groups form one or even two hydrogen bonds in the crystal. However, the similarity of the pH dependencies of RNase A inhibition by ppA-3′-p and by ppA-2′-p (R. Shapiro, unpublished observations) suggests that this linkage is weak.

Five of the eight water molecules present in the active site of the free RNase A structure are displaced upon binding of ppA-3′-p or ppA-2′-p; three lie in the region occupied by adenine, and two are near the position occupied by the pyrophosphate group. Those that remain form hydrogen bonds with N1 of adenine and with the pyrophosphate of each complex (Table 3). Some of these water molecules serve as bridges between the inhibitor and enzyme, connecting adenine N1 and Nδ2 of Asn 67 and pyrophosphate oxygens O1B and O3A with Nε2 of Gln 11.

Although the structures presented here are based on soaking experiments, data from RNase A cocrystallized with 0.5 mM ppA-3′-p were also available at 1.7 Å resolution. Preliminary analysis of this structure showed that the inhibitor is bound in exactly the same way as in the soaked crystal.

Modeling of Complexes of Angiogenin with ppA-3′-p and ppA-2′-p. The relevance of the present RNase complex structures for development of inhibitors of the related protein, human Ang, was examined by superimposing the Ang crystal structure (Acharya et al., 1994) with each complex and then performing energy minimization on the resultant Ang−inhibitor models. ppA-2′-p is the most effective nucleotide inhibitor of Ang identified thus far (Russo et al., 1996) and binds several-fold more tightly than the 3′ isomer (the opposite isomer is preferred by RNase A). However, the affinity of this compound for Ang is several hundred-fold lower than that for RNase A. Examination of the energy-minimized models indicates that both nucleotides can be accommodated in the Ang active site in the same orientation as for RNase A and there are no significant conflicts. Hydrogen bonds of the β-phosphate at P_1 and stacking interactions of adenine in the models correspond reasonably well with those in the RNase complexes, but the adenine forms only one hydrogen bond in the 2′-p complex, and none in the 3′-p complex. In both complexes, the monophosphate is within hydrogen bonding distance of Arg 5, which was demonstrated previously to be a functional component of the P_2 site (Russo et al., 1996). Thus, the modeled structures are consistent with the known kinetic properties of the inhibitors. However, a previous model of the complex of Ang with ppA-2′-p (Russo et al., 1996) in which the nucleotide is positioned in the standard conformation (i.e., with the 5′-α-phosphate in P_1) can also account for the kinetic findings. Structural studies on the complex of Ang with ppA-2′-p now in progress should reveal whether the inhibitor indeed binds as in either of these models.

Conclusions and Implications. The inhibitors ppA-3′-p and ppA-2′-p bind to RNase A more tightly than any other nucleotide reported to date. Their K_i values of 240 and 520 nM, respectively, are well below those of 2′-CMP (Anderson et al., 1968) and uridine vanadate (Lindquist et al., 1973), until now the most effective small-molecule inhibitors for which RNase A complex structures have been determined (Howlin et al., 1987; Wlodawer et al., 1983). In contrast to 2′-CMP and uridine vanadate, which interact with the B_1 and P_1 sites of RNase, the present inhibitors bind to the P_1/B_2/P_2 region. They do so in a highly unusual manner that requires them to adopt conformations markedly different from those observed for other occupants of these sites studied previously. Both inhibitors are anchored to RNase largely by extensive interactions that involve their most distant parts but are nonetheless interdependent. At one end, the 5′-β-phosphate forms four hydrogen bonds with P_1 site residues of RNase in much the same manner as does the 5′-α-phosphate in earlier complexes. At the other end, the adenine ring hydrogen bonds to Asn 71 and either Asn 67 or Gln 69, engages in π−π stacking interactions with His 119, and forms at least 17 van der Waals contacts with RNase. The interactions at each end restrict the possibilities at the other end and place constraints on the nucleotide conformation. Thus, with the 5′-β-phosphate placed at P_1, adenine cannot occupy B_2 unless the glycosyl torsion angle χ and the C4′/C5′ torsion angle γ are in the atypical *syn* and *−sc* ranges, respectively. Similarly, with adenine in a *syn* orientation at B_2, only the 5′-β-phosphate can extend fully into the P_1 site,

and it can do so only if the torsion angle γ lies in the $-sc$ range. The capacity of the adenine moiety to form productive interactions in both *syn* and *anti* orientations reflects the versatility of this purine and the adaptability of the B_2 site, some of whose residues shift in position by up to 2 Å in the various complexes.

Although the interactions of the 5′-β-phosphate and adenine with RNase A are largely similar in the ppA-3′-p and ppA- 2′-p complexes, those involving the intervening portions of the inhibitors differ in significant respects (Table 3). Most notably, in the 3′-p complex, the monophosphate appears to form a good hydrogen bond with Lys 7, whereas in the 2′-p complex, it does not interact strongly with the protein. This difference, however, translates into a disparity in binding energy of only 0.5 kcal/mol, perhaps because of the additional hydrogen bond between Lys 7 and the 5′-α-phosphate in the 2′-p complex.

The new RNase A complex structures presented here suggest several ways in which more potent RNase inhibitors might be constructed from the ppA-3′-p or ppA-2′-p nucleus. One of these is addition to the β-phosphate of a suitably linked substituent that would interact with B_1 site residues such as Thr 45, Phe 120, Ser 123, and Val 43. The 2′- and 3′-positions of the ribose may also be useful attachment points. The 2′-hydroxyl of ppA-3′-p is several angstroms from the side chain of Glu 111 and does not itself interact with RNase. Therefore, addition of a spacer-linked cationic group to O2′ or C2′ might improve binding. Modifications of the 3′-phosphate of this inhibitor might also introduce additional contacts, in this case with neighboring residues in the N-terminal segment of the protein.

Although the present structures provide a promising starting point for the rational design of tight-binding RNase inhibitors, they also reveal that this process may not follow a predictable course. Initial modeling of the ppA-3′-p complex from the d(ApTpApA)−RNase A crystal structure had suggested that the pAp portion of the new inhibitor could bind at P_1, B_1, and P_2 in the same way as the corresponding part of the tetranucleotide and that the β-5′-phosphate would interact favorably with residues adjacent to the P_1 site. This binding mode was not altered significantly by energy minimization with X-PLOR (Brünger, 1992a). Nonetheless, as we have shown, the actual complex structure is quite different. The marked difference in the ribose conformations in the ppA-3′-p and ppA-2′-p complexes was also unexpected, and is not a simple reflection of the propensities of the unbound inhibitors (Altona & Sundaralingam, 1972). Thus, it appears that even small modifications of the inhibitor's chemical structure can generate profound alterations in its mode of interaction with the target protein. Similar phenomena have been encountered previously in the design of inhibitors of HIV protease (Reich et al., 1995) and stromelysin (Rockwell et al., 1996). These findings emphasize the importance of obtaining direct structural information on each new inhibitor complex on the optimization pathway.

ACKNOWLEDGMENT

We are grateful to the staff at the Synchrotron Radiation Source at Daresbury, England, to the staff of HASYLAB, at the EMBL outstation of DESY Hamburg, Germany, and to A. C. Papageorgiou for help with X-ray data collection. We thank Drs. James F. Riordan and Bert L. Vallee for advice and support.

REFERENCES

Acharya, K. R., Shapiro, R., Allen, S. C., Riordan, J. F., & Vallee, B. L. (1994) *Proc. Natl. Acad. Sci. U.S.A. 91*, 2915−2919.
Altona, C., & Sundaralingam, M. (1972) *J. Am. Chem. Soc. 94*, 8205−8212.
Anderson, D. G., Hammes, G. G., & Walz, F. G. (1968) *Biochemistry 7*, 1637−1645.
Bailey, S. (1994) *Acta Crystallogr. D 50*, 760−763.
Blackburn, P., & Moore, S. (1982) *The Enzymes 15*, 317−433.
Borkakoti, N., Moss, D. A., & Palmer, R. A. (1982) *Acta Crystallogr. B 38*, 2210−2217.
Brünger, A. T. (1992a) *X-PLOR Version 3.1 Manual: A system for X-ray Crystallography & NMR*, Yale University Press, New Haven, CT.
Brünger, A. T. (1992b) *Nature 355*, 472−475.
Burley, S. K., & Petsko, G. A. (1988) *Adv. Protein Chem. 39*, 124−189.
D'Alessio, G. (1993) *Trends Cell Biol. 3*, 106−109.
deMel, S. J., Doscher, M. S., Martin, P. D., Rodier, F., & Edwards, B. F. P. (1995) *Acta Crystallogr. D 51*, 1003−1012.
Eftink, M. E., & Biltonen, R. L. (1987) in *Hydrolytic Enzymes*, pp 333−376, Elsevier Science Publishers, Amsterdam, New York, and Oxford.
Fett, J. W., Strydom, D. J., Lobb, R. R., Alderman, E. M., Bethune, J. L., Riordan, J. F., & Vallee, B. L. (1985) *Biochemistry 24*, 5480−5486.
Filman, D. J., Bolin, J. T., Matthews, D. A., & Kraut, J. (1982) *J. Biol. Chem. 257*, 13663−13672.
Fontecilla-Camps, J. C., de Llorens, R., le Du, M. H., & Cuchillo, C. M. (1994) *J. Biol. Chem. 269*, 21526−21531.
French, S., & Wilson, K. S. (1978) *Acta Crystallogr. A 34*, 517−525.
Gleich, G. J., Loegering, D. A., Bell, M. P., Checkel, J. L., Ackerman, S. J., & McKean, D. J. (1986) *Proc. Natl. Acad. Sci. U.S.A. 83*, 3146−3150.
Hodel, A., Kim, S.-H., & Brünger, A. T. (1992) *Acta Crystallogr. A 48*, 851−859.
Howlin, B., Harris, G. W., Moss, D. S., & Palmer, R. A. (1987) *J. Mol. Biol. 196*, 159−164.
Howlin, B., Moss, D. S., & Harris, G. W. (1989) *Acta Crystallogr. A 45*, 851−861.
Irie, M., Watanabe, H., Ohgi, K., Tobe, M., Matsumura, G., Arata, Y., Hirose, T., & Inayama, S. (1984) *J. Biochem. 95*, 751−759.
IUPAC-IUB Joint Commission on Biochemical Nomenclature (1983) *Eur. J. Biochem. 131*, 9−15.
Jones, T. A., Zou, J. Y., Cowan, S. W., & Kjeldgaard, M. (1991) *Acta Crystallogr. A 47*, 110−119.
Kabsch, W. (1988) *J. Appl. Crystallogr. 21*, 916−924.
Kim, E. E., Varadarajan, R., Wyckoff, H. W., & Richards, F. M. (1992) *Biochemistry 31*, 12304−12314.
Kraulis, P. J. (1991) *J. Appl. Crystallogr. 24*, 946−950.
Laskowski, R. A., MacArthur, M. W., Moss, D. S., & Thornton, J. M. (1993) *J. Appl. Crystallogr. 26*, 283−291.
Lindquist, R. N., Lynn, J. L., & Lienhard, G. E. (1973) *J. Am. Chem. Soc. 95*, 8762−8768.
Lisgarten, J. N., Gupta, V., Maes, D., Wyns, L., Zegers, I., Palmer, R. A., Dealwis, C. G., Aguilar, C. F., & Hemmings, A. M. (1993) *Acta Crystallogr. D49*, 541−547.
Moodie, S. L., & Thornton, J. M. (1993) *Nucleic Acids Res. 21*, 1369−1380.
Mosimann, S. C., Newton, D. L., Youle, R. J., & James, M. N. G. (1996) *J. Mol. Biol. 260*, 540−552.
Navaza, J. (1994) *Acta Crystallogr. A 50*, 157−163.
Olson, K. A., French, T. C., Vallee, B. L., & Fett, J. W. (1994) *Cancer Res. 54*, 4576−4579.
Olson, K. A., Fett, J. W., French, T. C., Key, M. E., & Vallee, B. L. (1995) *Proc. Natl. Acad. Sci. U.S.A. 92*, 442−446.
Otwinowski, Z. (1993) in *Data Collection and Processing* (Sawyer, L., Isaacs, N., & Bailey, S. S., Eds.) pp 56−62, SERC Daresbury Laboratory, Warrington, UK.

Parés, X., Nogués, M. V., Llorens, R., & Cuchillo, C. M. (1991) *Essays Biochem. 26*, 89−103.
Read, J. (1986) *Acta Crystallogr. A 42*, 140−149.
Reich, S. H., Melnick, M., Davies, J. F., Appelt, K., Lewis, K. K., Fuhry, M. A., Pino, M., Trrippe, A. J., Nguyen, D., Dawson, H., Wu, B. W., Musick, L., Kosa, M., Kahil, D., Webber, S., Gehlhaar, D. K., Andrada, D., & Shetty, B. (1995) *Proc. Natl. Acad. Sci. U.S.A. 92*, 3298−3302.
Richards, F. M., & Wyckoff, H. W. (1971) *The Enzymes 4*, 647−806.
Richards, F. M., Wyckoff, H. W., Carlson, W. D., Allewell, N. M., Lee, B., & Mitsui, Y. (1972) *Cold Spring Harbor Symp. Quant. Biol. 36*, 35−43.
Rockwell, A., Melden, M., Copeland, R. A., Hardman, K., Decicco, C. P., & DeGrado, W. F. (1996) *J. Am. Chem. Soc. 118*, 10337−10338.
Russo, N., Acharya, K. R., Vallee, B. L., & Shapiro, R. (1996) *Proc. Natl. Acad. Sci. U.S.A. 93*, 804−808.
Russo, N., Shapiro, R., & Vallee, B. L. (1997) *Biochem. Biophys. Res. Commun. 231*, 671−674.
Shapiro, R., & Vallee, B. L. (1989) *Biochemistry 28*, 7401−7408.
Shapiro, R., Fox, E. A., & Riordan, J. F. (1989) *Biochemistry 28*, 1726−1732.
Sorrentino, S., Glitz, D. G., Hamann, K. J., Loegering, D. A., Checkel, J. L., & Gleich, G. L. (1992) *J. Biol. Chem. 267*, 14859−14865.
Strydom, D. J., Fett, J. W., Lobb, R. R., Alderman, E. M., Bethune, J. L., Riordan, J. F., & Vallee, B. L. (1985) *Biochemistry 24*, 5486−5494.
Toiron, C., Gonzalez, C., Bruix, M., & Rico, M. (1996) *Protein Sci. 5*, 1633−1647.
Williams, R. L., Greene, S. M., & McPherson, A. (1987) *J. Biol. Chem. 262*, 16020−16031.
Wlodawer, A., Miller, M., & Sjolin, L. (1983) *Proc. Natl. Acad. Sci. U.S.A. 80*, 3628−3631.
Wlodawer, A., Svensson, L. A., Sjolin, L., & Gilliland, G. L. (1988) *Biochemistry 27*, 2705−2717.
Zegers, I., Maes, D., Dao-Thi, M.-H., Poortmans, F., Palmer, R., & Wyns, L. (1994) *Protein Sci. 31*, 2322−2339.

BI9700330